Stratospheric ozone over the United States in summer linked to observations of convection and temperature via chlorine and bromine catalysis

James G. Anderson[a,b,c,1], Debra K. Weisenstein[c], Kenneth P. Bowman[d], Cameron R. Homeyer[e], Jessica B. Smith[c], David M. Wilmouth[a,c], David S. Sayres[c], J. Eric Klobas[a], Stephen S. Leroy[c], John A. Dykema[c], and Steven C. Wofsy[b,c]

[a]Department of Chemistry and Chemical Biology, Harvard University, Cambridge, MA 02138; [b]Department of Earth and Planetary Sciences, Harvard University, Cambridge, MA 02138; [c]Harvard John A. Paulson School of Engineering and Applied Sciences, Harvard University, Cambridge, MA 02138; [d]Department of Atmospheric Sciences, Texas A&M University, College Station, TX 77843; and [e]School of Meteorology, University of Oklahoma, Norman, OK 73019

Edited by John H. Seinfeld, California Institute of Technology, Pasadena, CA, and approved May 9, 2017 (received for review November 28, 2016)

We present observations defining (*i*) the frequency and depth of convective penetration of water into the stratosphere over the United States in summer using the Next-Generation Radar system; (*ii*) the altitude-dependent distribution of inorganic chlorine established in the same coordinate system as the radar observations; (*iii*) the high resolution temperature structure in the stratosphere over the United States in summer that resolves spatial and structural variability, including the impact of gravity waves; and (*iv*) the resulting amplification in the catalytic loss rates of ozone for the dominant halogen, hydrogen, and nitrogen catalytic cycles. The weather radar observations of ∼2,000 storms, on average, each summer that reach the altitude of rapidly increasing available inorganic chlorine, coupled with observed temperatures, portend a risk of initiating rapid heterogeneous catalytic conversion of inorganic chlorine to free radical form on ubiquitous sulfate–water aerosols; this, in turn, engages the element of risk associated with ozone loss in the stratosphere over the central United States in summer based upon the same reaction network that reduces stratospheric ozone over the Arctic. The summertime development of the upper-level anticyclonic flow over the United States, driven by the North American Monsoon, provides a means of retaining convectively injected water, thereby extending the time for catalytic ozone loss over the Great Plains. Trusted decadal forecasts of UV dosage over the United States in summer require understanding the response of this dynamical and photochemical system to increased forcing of the climate by increasing levels of CO_2 and CH_4.

stratospheric ozone | climate change | UV radiation human health effects | convection | water vapor

An array of recent observational evidence has brought renewed focus on the dynamical and photochemical mechanisms that control ozone in the lower stratosphere over the United States in summer. In particular, the coupling of five factors, when considered in specific combinations, define why the central United States in summer represents a unique case, in the global context, for the risk of regional ozone loss. These factors, depicted in Fig. 1, include (*i*) development of severe storm systems over the Great Plains of the United States with convective cores that extend well above the tropopause, leading to the injection of water vapor and possibly halogen radical precursors deep into the stratosphere (1–5); (*ii*) anticyclonic flow in the stratosphere over the United States in summer, associated with the North American monsoon (NAM), that serves to increase the retention time of the convectively injected species over the United States (6, 7); (*iii*) increased probability for the catalytic conversion of inorganic chlorine (primarily HCl and $ClONO_2$, hereafter Cl_y) to free radical form (ClO) on ubiquitous sulfate aerosols due to a combination of ambient temperature perturbations and localized water vapor enhancements, which can accelerate the catalytic removal of ozone in the lower stratosphere (2, 8); (*iv*) potential for future sulfate enhancements from volcanic eruptions (9–12) or overt addition by the geoengineering approach of reducing solar forcing by increasing albedo via solar radiation management (SRM) (13–18); and (*v*) increased forcing of the climate by continued CO_2 and CH_4 emissions, from the extraction, transport, and combustion of fossil fuels, that has the potential to increase the frequency and intensity of storm systems over the Great Plains in summer (19–22).

The objectives of this paper are to: (*i*) show the frequency and depth of convective penetration into the stratosphere of condensed phase water over the central United States in summer using observations from the Next-Generation Radar (NEXRAD) weather radar system; (*ii*) present available inorganic chlorine within the same vertical coordinate system as the NEXRAD observations; (*iii*) present high-accuracy, high resolution in situ observations of the temperature structure of the lower stratosphere over the United States in summer that clarify the importance of spatial and structural variability and gravity wave propagation on the heterogeneous catalytic conversion of inorganic chlorine to free radical form; and (*iv*) use the observations of convective penetration heights, elevated water vapor, and temperatures as inputs to the Atmospheric and Environmental Research (AER) 2D model (10, 23–26), which calculates concentrations of the rate-limiting ClO, BrO, HO_2, and NO_2 radicals that control the catalytic loss rate of ozone and the resulting fractional decrease in ozone.

The context for the analysis presented here concerns the issue of human health associated with the remarkable sensitivity of humans to small increases in UV dosage that initiate skin cancer. In particular, diagnosed cases of basal cell and squamous cell carcinoma have reached 3.5 million annually in the United States alone (27–31). The analysis presented here of the sensitivity of

Significance

Stratospheric ozone is one of the most delicate aspects of habitability on the planet. Removal of stratospheric ozone over the polar regions in winter/spring has established the vulnerability of ozone to halogen catalytic cycles. Elevated ClO concentrations engendered, in part, by heterogeneous catalytic conversion of inorganic chlorine to free radical form on ubiquitous sulfate–water aerosols, govern the rate of ozone removal. We report here observations of the frequency and depth of penetration of convectively injected water vapor into the stratosphere, triggered by severe storms that are specific to the central United States in summer, and model their effect on lower stratospheric ozone. This effect implies, with observed temperatures, increased risk of ozone loss over the Great Plains in summer.

Author contributions: J.G.A. designed research; J.G.A. and D.K.W. performed research; D.K.W., K.P.B., C.R.H., J.B.S., D.M.W., D.S.S., J.E.K., S.S.L., J.A.D., and S.C.W. analyzed data; J.G.A. wrote the paper; K.P.B. and C.R.H. contributed NEXRAD data; and J.B.S., D.M.W., and D.S.S. contributed in situ data.

The authors declare no conflict of interest.

This article is a PNAS Direct Submission.

[1]To whom correspondence should be addressed. Email: anderson@huarp.harvard.edu.

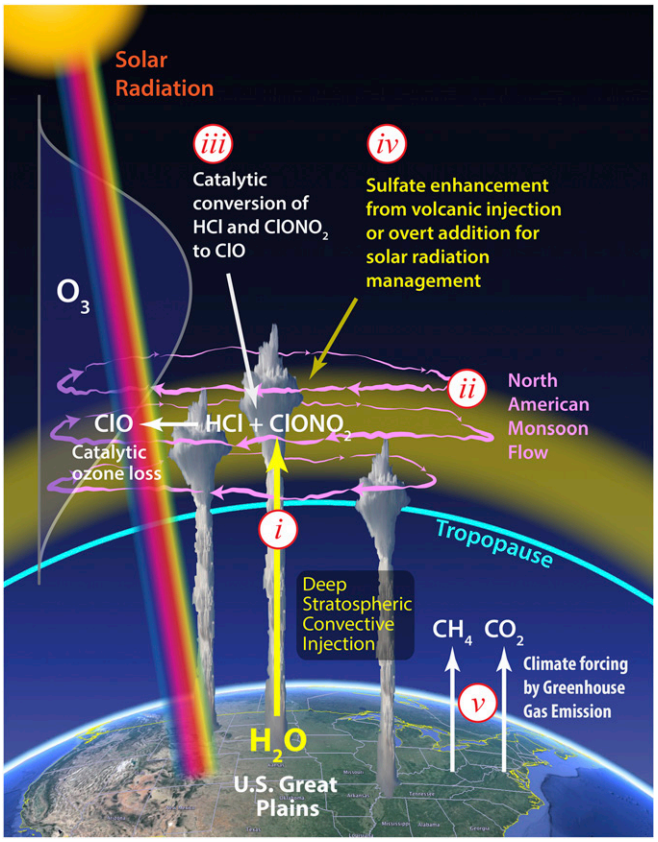

Fig. 1. In the context of climate–chemistry coupling globally, the central United States in summer represents a combination of factors specific to both the geographic region and the season. Northerly flow of warm moist air from the Gulf of Mexico in combination with heating and convergence over the Great Plains frequently triggers powerful convection that injects water vapor into the stratosphere, where the upper level anticyclonic flow associated with the NAM can sequester the injection for up to a week or more over the United States. These conditions, in combination with cold stratospheric temperatures, can lead to heterogeneous catalysis on ubiquitous sulfate–water aerosols that converts inorganic chlorine to ClO and can initiate ozone loss through an array of gas-phase catalytic cycles. Potential future enhancements in sulfate from volcanic injection or geoengineering increase the likelihood of halogen activation and ozone loss.

lower stratospheric ozone over the United States in summer builds on four decades of developments linking chlorine and bromine radicals to ozone loss in the polar regions (e.g., refs. 32–43), ozone depletion at midlatitudes resulting from the coupling of volcanic aerosols and temperature variability to anthropogenic chlorine and bromine (8, 10, 11, 44), and analyses of the consequences from sulfate addition to the stratosphere from geoengineering via SRM (15–18). Finally, although detailed simultaneous observations of the key catalytic free radicals, reactive intermediates, and ozone loss rates have been thoroughly investigated in the stratosphere over the Antarctic and Arctic in winter, the same is not the case for the stratosphere over the United States in summer.

Advances in Stratospheric Observations

Photochemical Framework for Catalytic Ozone Loss in the Lower Stratosphere. Studies of catalytic ozone loss in the lower stratosphere at high latitudes established the network of catalytic reactions linking inorganic chlorine to the rate of ozone loss in the lower stratosphere. Simultaneous in situ aircraft observations of ClO, BrO, ClOOCl, $ClONO_2$, HCl, OH, HO_2, NO_2, particle surface area, H_2O, and O_3 in the transition through the boundary of the Arctic vortex (38–42) showed explicitly the loss of ozone as well as the distinct anticorrelation between the concentration of the rate-limiting radical ClO and the ozone concentration. It is the chlorine monoxide radical, ClO, in combination with the rate-limiting step ClO + ClO + M → ClOOCl + M in the catalytic cycle first introduced by Molina and Molina (34) and the catalytic cycle rate limited by ClO + BrO → Cl + Br + O_2 first introduced by McElroy et al. (35) that constitute the reaction mechanisms capable of removing ozone over the polar regions in winter at the observed rates (36, 41, 42).

A distinguishing feature of the regime within the polar jet, which defines the boundary of the Arctic vortex in winter, is that temperatures within the vortex are lower by ∼6 K to 7 K than outside the vortex. This modest suppression in temperature is adequate to trigger the heterogeneous catalytic conversion of Cl_y to Cl_2 and HOCl at H_2O mixing ratios of 4.5 parts per million by volume (ppmv) on simple, ubiquitous sulfate aerosols (8, 45–48) via the three reactions displayed in the upper left of Fig. 2. The Cl_2 and HOCl products of Cl_y heterogeneous catalysis on sulfate aerosols (33) photodissociate to produce Cl atoms that react with O_3 to produce ClO. Hereafter, we refer to this series of reactions as the conversion of Cl_y to ClO.

Examination of conditions in the Arctic lower stratosphere coupled with extensive results from laboratory experiments and modeling (45–48) have set in place the temperature–water vapor–sulfate coordinate system defining the regime of rapid heterogeneous conversion of Cl_y to ClO (2). Fig. 2 displays a schematic illustrating the temperature–water vapor threshold between the domain in which conversion of inorganic chlorine to its catalytically active forms becomes significant (shaded region) and the temperature–water vapor domain that leaves inorganic chlorine bound in its reservoir species (unshaded region) (45–48). Probabilities (γ) associated with the heterogeneous reactions considered here are sensitive to aerosol composition (45–48). In particular, reactions involving HCl are governed by its uptake

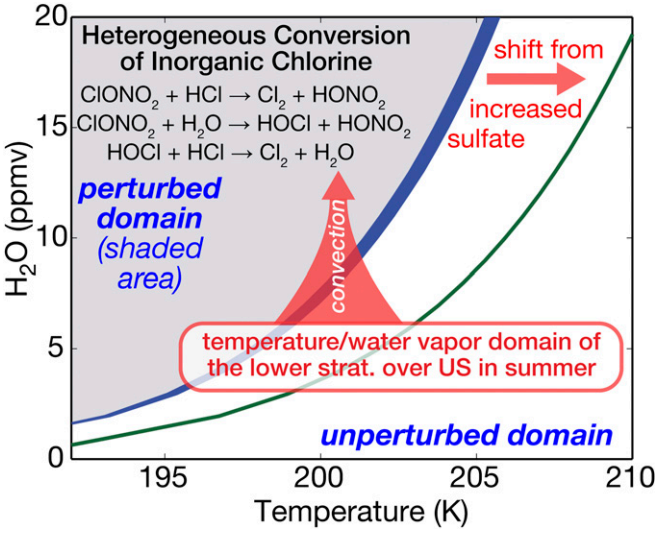

Fig. 2. An example of the dependence of heterogeneous catalytic conversion of inorganic chlorine ($Cl_y \approx HCl + ClONO_2$) on temperature, water vapor, and sulfate loading is displayed in a manner that distinguishes rapid conversion of Cl_y to free radical form in the shaded region (with the threshold defined as 10% chlorine activation in the first diurnal period) from the unshaded region for which there is virtually no Cl_y to ClO conversion. These domains establish the photochemical framework for the analysis of convective addition of water, sulfate addition by volcanic injection or overt sulfate addition for SRM, or combinations thereof. The broad blue line dividing the perturbed and unperturbed domains corresponds to a sulfate reactive surface area of 2 $\mu m^2/cm^3$; the green line represents a shift in sulfate reactive surface area to 20 $\mu m^2/cm^3$.

and solubility, which are strongly dependent on both the sulfuric acid weight percent of the aerosol and temperature. As the sulfuric acid weight percent decreases, the solubility of HCl increases. The sulfuric acid weight percent is itself a function of relative humidity. With shifts to colder temperatures and/or higher water vapor mixing ratios leading to more dilute sulfate within the aerosol, the reaction probabilities for the conversion of Cl_y to ClO increase exponentially. Therefore, wherever the specific conditions of temperature and water vapor are satisfied, the heterogeneous catalytic conversion of Cl_y to ClO can occur on the simple, ubiquitous binary aerosol, and ozone loss can result.

The cornerstone of our understanding of sulfate–halogen-induced reductions in ozone over midlatitudes of the Northern Hemisphere (NH) is built upon observed column ozone loss following the 1991 eruption of Mount Pinatubo (8, 10–12). The impact of the volcanic eruption on ozone extended over a period of nearly 4 y following the eruption when column ozone concentrations over the NH decreased by a maximum of 5% in the latitude region 35°N to 60°N (10). Model analysis of the impact emphasized the central role of halogen radical catalytic loss of ozone, particularly the important role of bromine radicals in the lower stratosphere at elevated levels of sulfate aerosol loading (10). The addition of sulfate to the stratosphere by either volcanic injection or overt addition for SRM is indicated in Fig. 2 as the sulfate "shift" to the green line that serves to move the domain for rapid heterogeneous catalytic conversion of Cl_y to ClO.

The four catalytic cycles that must be taken into account in the assessment of ozone loss rates in the lower stratosphere include the most important rate-limiting steps under unperturbed as well as perturbed conditions, i.e., conditions of elevated water vapor or lower temperatures. In this analysis, unperturbed refers to background sulfate loading of 1 $\mu m^2/cm^3$ to 3 $\mu m^2/cm^3$ and a water vapor mixing ratio of 4.5 ppmv. The four dominant rate-limiting catalytic steps include (*i*) $ClO + ClO + M \rightarrow ClOOCl + M$, (*ii*) $BrO + ClO \rightarrow Br + Cl + O_2$, (*iii*) $NO_2 + O \rightarrow NO + O_2$, and (*iv*) $HO_2 + O_3 \rightarrow OH + 2O_2$. Under unperturbed conditions in the lower stratosphere between 10 km and 22 km, the catalytic loss of ozone is dominated by the $HO_2 + O_3 \rightarrow OH + 2O_2$ rate-limiting step, as originally demonstrated by Wennberg et al. (49). The ClO + BrO cycle plays a significant role (~15%), exceeding the ClO dimer catalytic cycle by more than an order of magnitude under unperturbed conditions. Above ~22 km, the catalytic cycle rate limited by $NO_2 + O \rightarrow NO + O_2$ becomes dominant. The rate-limiting catalytic species ClO, BrO, HO_2, and NO_2 thus constitute the baseline against which unperturbed conditions may be contrasted relative to perturbed cases involving temperature variability and the convective injection of water vapor.

NEXRAD Weather Radar Map of Storm-Top Height Geographic Distribution and Penetration Depth into the Stratosphere over the United States in Summer. The NEXRAD weather radar network has markedly advanced our understanding of both the frequency and depth of tropopause-penetrating convection in the lower stratosphere over the United States in summer. Before the radar analysis methods developed by Homeyer (50) and applied by Solomon et al. (51) for mapping the 3D structure of convective penetration, elevated water vapor mixing ratios in the stratosphere were observed in situ during multiple summertime aircraft missions over the United States (1, 2, 52). These observations of both vapor-phase H_2O and the HDO isotopologue, obtained aboard NASA's WB-57 and ER-2 aircraft, provide direct evidence of water vapor deposited by convection in the stratosphere. Maximum water vapor values observed in situ range from 8 ppmv to 18 ppmv for individual plumes typically sampled a day to a few days after convective injection. In support of the in situ observations, the NEXRAD weather radar data provide compelling statistics on the frequency, 3D structure, and high accuracy determination of the storm-top altitude of convection.

Solomon et al. (51) used radar analysis methods developed by Homeyer (50) and observations from the operational NEXRAD radar network to create a high-resolution, 3D, gridded radar reflectivity product for 2004 over the conterminous United States east of the Rocky Mountains. By combining the NEXRAD analysis with the lapse-rate tropopause height derived from the interim reanalysis of the European Centre for Medium-Range Weather Forecasts (ERA-Interim), they produced high-resolution maps of convection overshooting the tropopause level at 3-h intervals for the entire year. The ERA-Interim estimates of the tropopause altitude agree well with high vertical resolution observations from radiosondes (53). These ice-rich overshooting parcels lead to injection of water vapor into the stratosphere through mechanisms including turbulent mixing and gravity wave breaking (53, 54).

The geographic distribution of overshooting events is markedly nonuniform, with the great majority occurring east of the Rocky Mountains and west of the Mississippi River, as presented in Fig. 3*A*. The largest concentration of overshooting events occurs over the high plains stretching from Texas to Nebraska and Iowa. The ongoing analysis of a 10-y hourly NEXRAD dataset for May through August of 2004–2013 confirms the diurnal, annual, and geographical patterns found by Solomon et al. (51). A key contribution that the NEXRAD system provides is the ability to map the storm-top potential temperature as a function of geographic position, frequency, and month of occurrence. The multiyear analysis indicates that 38,158 storms reached at least 2 km above the tropopause over the central United States in May–August between 2004 and 2013, with about 50% of these extending above the 390 K potential temperature level. The depth and frequency of penetration has significant consequences, so we delineate here the quantitative specifics of the NEXRAD observations with high spatial resolution values of HCl that inform the altitude-dependent distribution of available inorganic chlorine.

The vertical coordinate system most appropriate for the quantitative coupling of the NEXRAD observations to that of inorganic chlorine is potential temperature (the temperature of an air parcel compressed adiabatically to 1,000 hPa) because, in the absence of diabatic processes, air parcels in the stratosphere are transported along surfaces of constant potential temperature, such that long-lived trace species exhibit consistent correlations with one another. In particular, this is a characteristic shared by long-lived tracers that are either produced or removed by increasing UV radiation as a function of increasing altitude in the stratosphere, e.g., HCl vs. O_3 and Cl_y vs. N_2O. Data from multiple in situ measurement campaigns, as well as satellite retrievals, have been used to quantify the relationships among these species (42, 55, 56). In Fig. 3*B*, high-resolution vertical profiles of HCl mixing ratio (blue and red circles) were inferred from in situ measurements of O_3 using the linear relationship between Aura Microwave Limb Sounder (MLS) measurements of HCl and O_3 at 100 hPa and 68 hPa, such that $HCl \approx 7.0 \times 10^{-4} \times O_3$ (units of parts per trillion by volume). MLS version 4.2 data from 2004 to 2016, subselected to be between 30°N to 50°N and 80°W to 105°W for June through August, were used to derive this conversion factor. The in situ O_3 data used to calculate HCl throughout the lower stratosphere over the United States in summer are from the NASA Studies of Emissions and Atmospheric Composition, Clouds, and Climate Coupling by Regional Surveys ($SEAC^4RS$) mission, which took place over the United States in the summer of 2013. Also shown in Fig. 3*B* are in situ measurements of HCl from the NASA Aura Validation Experiment (AVE) campaign over the United States in June 2005 and bin-averaged satellite measurements of HCl from MLS over the United States in summer as a function of potential temperature. The dotted lines define 1 SD from the mean of the MLS HCl data. The in situ and satellite measurements of HCl support the more complete vertical profiles of inferred HCl that are used subsequently to compare with NEXRAD data. HCl comprises

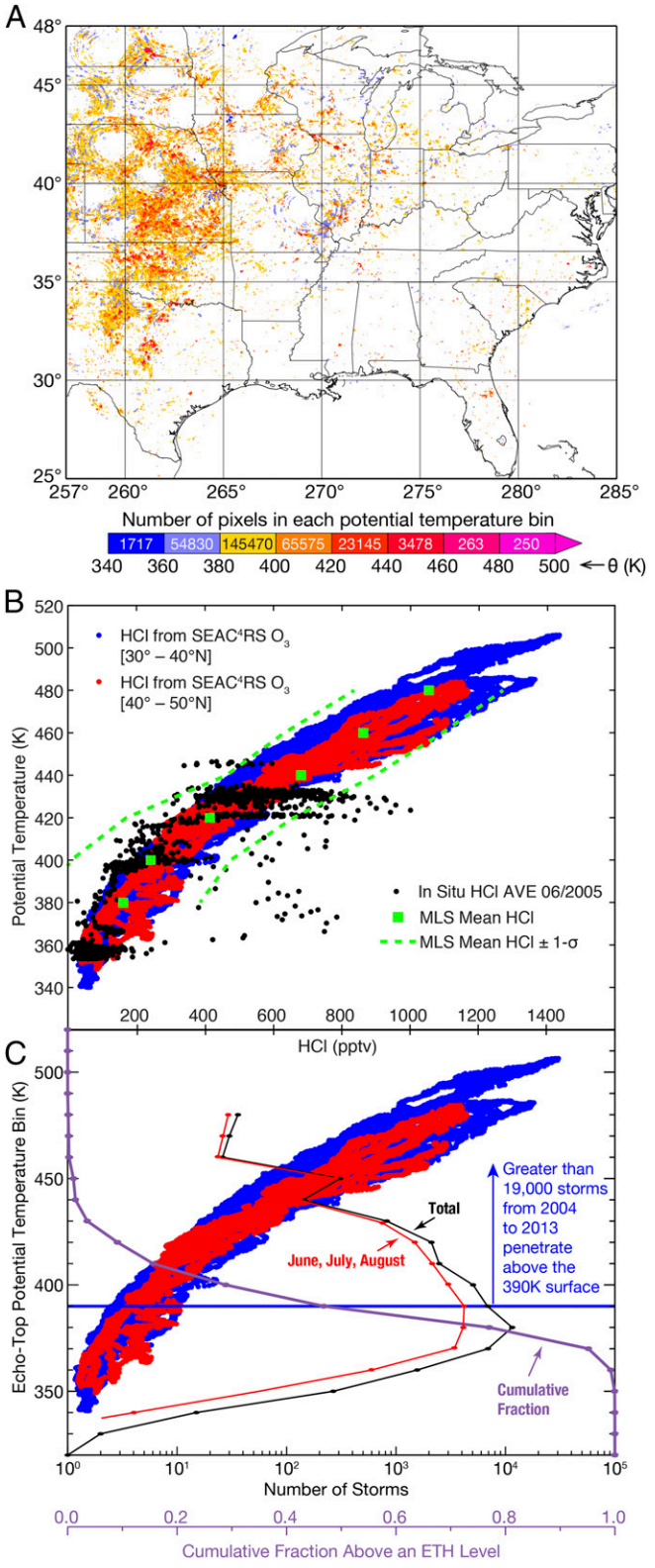

Fig. 3. (*A*) The geographic distribution of deep stratospheric convective injection from the NEXRAD weather radar 3D mapping of storms in the summer (May–August 2004–2013) that penetrate more than 2 km above the local tropopause. (*B*) The vertical distribution of inferred HCl as a function of potential temperature in the stratosphere over the United States in summer for two latitude bins (blue and red points), where HCl is calculated using in situ O_3 data from the NASA SEAC^{4}RS mission. In situ measurements acquired by the National Oceanic and Atmospheric Administration chemical ionization mass spectrometer (CIMS) HCl instrument during the NASA AVE mission in June 2005 are included for comparison with the inferred HCl. Data acquired between 30°N to 50°N and 80°W to 105°W are shown. Also plotted are bin-averaged measurements of HCl acquired by MLS as a function of potential temperature, calculated from simultaneous measurements of temperature at the 100- and 68-hPa pressure levels (green squares). The dashed green lines indicate the range 1 SD from the mean for each 20 K potential temperature bin. The MLS satellite data were selected to be between 30°N to 50°N and 80°W to 105°W for June–August from 2004 to 2016. (*C*) The total number of storms that penetrate more than 2 km into the stratosphere over the central United States in May–August (black) and June–August (red) from 2004 to 2013 as a function of potential temperature. The calculated HCl mixing ratio is superimposed on the NEXRAD observations of frequency and penetration height.

most of the inorganic chlorine in the lower stratosphere, and, accordingly, Fig. 3*B* demonstrates the rapid rise in available inorganic chlorine with increasing potential temperature (altitude).

Fig. 3*C* displays the NEXRAD observations of convective injection as a function of potential temperature, showing the total number of storms observed in the summer (May–August) between 2004 and 2013, and the number of those storms that occurred in June, July, and August. Of particular importance is the fact that more than 50% of the observed 38,158 storms between 2004 and 2013 that reached 2 km above the tropopause penetrated above the 390 K potential temperature level. This height corresponds to the altitude of rapid increase in available inorganic chlorine. The vertical distribution of HCl is shown with the NEXRAD observations in the same coordinate system of potential temperature, which provides for the direct comparison of (*i*) convective penetration height and frequency with (*ii*) HCl, a lower limit on available inorganic chlorine, Cl_y.

Subsequent to the high in situ water vapor observations reported by Anderson et al. (2), Schwartz et al. (57) analyzed satellite observations of water vapor from MLS and confirmed that the lower stratosphere over the United States in summer is, indeed, unusually wet, with measured values reaching as high as 18 ppmv. The MLS satellite data indicate that the highest stratospheric water vapor mixing ratios at the highest latitudes globally are over the central and eastern United States in summer. These results are particularly noteworthy, because the true magnitude and number of water vapor enhancements over the United States in summer is likely significantly greater than reported by the MLS satellite instrument. This discrepancy occurs because elevated H_2O from convective injection is localized in space and typically layered vertically, such that the spatial resolution of MLS (e.g., 3 km vertical × 200 km horizontal at 100 hPa for H_2O) may often exceed the dimensions of the perturbation or randomly transect it, leading to an underestimate of the mixing ratio. For example, a 2-km-deep layer of elevated water of 50-km horizontal extent, even with optimal alignment of the convected geometry along the north–south viewing track of MLS, will only fill 1/6 of the MLS sample volume, with the other 5/6 filled with background levels of H_2O; this results in a substantial underreporting of the actual H_2O mixing ratio present within the convected domain. Nevertheless, Schwartz et al. (57) established the crucial fact that the stratosphere over the central and eastern United States is unique globally with respect to significantly elevated water vapor.

Another key piece of evidence relating the observations of enhanced water vapor to their convective source comes from the atmospheric chemistry experiment-Fourier transform spectrometer (ACE-FTS) satellite observations of the concentration of the heavy water isotopologue HDO globally in the lower stratosphere (58) as well as in situ observations of HDO within regions of convective injection from NASA aircraft missions (1). The HDO to H_2O ratio is expressed in the usual isotopic formulation of δD that is reported

in per mil units and defined as $\delta D(‰) = (R_{obs}/R_{SMOW} - 1) \times 1{,}000$, where $R = [HDO]/[H_2O]$, "SMOW" refers to standard mean ocean water, and $R_{SMOW} = 3.12 \times 10^{-4}$. Observations of δD are important because convective injection followed by sublimation is characterized by less negative values of δD in water vapor compared with air that has passed through the tropical tropopause, which has δD values of around −650‰. This number corresponds to a 65% depletion of HDO relative to SMOW. In situ aircraft measurements of convective outflow show δD values of −200‰ (1, 59). The ACE-FTS global observations of δD at 16.5 km from Randel et al. (58) show δD values of approximately −490‰ over North America in summer but virtually no enhancement of δD over the global mean at 16.5 km altitude in any other geographic domain, including the Asian monsoon region. These measurements provide direct evidence for the convective source of water vapor in the stratosphere over the United States in summer as well as for the unique occurrence of deep stratosphere-penetrating convection in the global context.

Observations of Temperatures in the Lower Stratosphere over the United States in Summer. We use high spatial resolution, high-accuracy in situ temperature measurements acquired in the specific altitude, latitude, longitude, and season appropriate for calculations of localized ozone loss in the lower stratosphere over the central United States in summer. These temperature data were acquired aboard the NASA ER-2 high-altitude aircraft on flights in the stratosphere during August and September 2013 over the central United States during the NASA SEAC^{4}RS mission. For the present analysis, which focuses specifically on the central United States east of the Rocky Mountains, we select temperature data in the latitude range from 30°N to 40°N and in longitude from 105°W to 80°W. The observed temperatures from the aircraft in situ measurements are displayed as the gray dots in Fig. 4. For comparison, Fig. 4 also shows the temperature profile from a 13-y record (2002–2014) of gridded, monthly average radio occultation (RO) observations from 30°N to 40°N for July and August, referred to hereafter as T_{RO}. Although not equal in spatial resolution to the in situ observations, the RO data provide an independent measure of the average temperature for this region and season, with an accuracy (absolute) of 0.1 K and spatial resolution of ∼0.5 km in the vertical (60, 61).

In the following modeling analysis, three different temperature profiles (Fig. 4) are used to evaluate the response of the rate-limiting steps for the catalytic loss of stratospheric ozone to temperature in both the presence and absence of convectively injected water vapor. The three temperature profiles are T_{std}, the AER 2D model "standard atmosphere" temperature (10, 23–26) profile, for the month of July; T_{ave}, a profile of the observed average temperatures with altitude, drawn from the SEAC^{4}RS in situ aircraft measurements; and T_{mid}, a temperature profile that lies at the midpoint between T_{ave} and the envelope of observed minimum temperatures from the in situ aircraft measurements. Inspection of the temperature profiles presented in Fig. 4 reveals the similarity between T_{ave} and T_{RO}. The difference, ∼1 K to 2 K in the altitude region from 14 km to 20 km, results from the fact that we are using monthly and spatially averaged (5° × 5° × ∼1 km) RO data. However, the agreement between T_{ave} from the in situ aircraft observations and T_{RO} from the RO observations serves as an important cross-calibration between these two physically independent absolute temperature measurements.

As Fig. 4 makes clear, there is a significant range in observed temperatures in the lower stratosphere over the central United States in summer. Spatial and structural variability in combination with gravity waves that continuously traverse the lower stratosphere over the Great Plains in summer contribute to the observed temperature variability. These gravity waves are induced by strong convective events embedded in mesoscale convective systems, squall lines and tornadic storm structures, as well as the presence of the Rocky Mountains (62–64). Also potentially contributing to the temperatures in the domain of elevated water vapor from convective injection is the radiative cooling to space at a rate of ∼0.05 K/d per 1 ppmv of additional water vapor (65, 66).

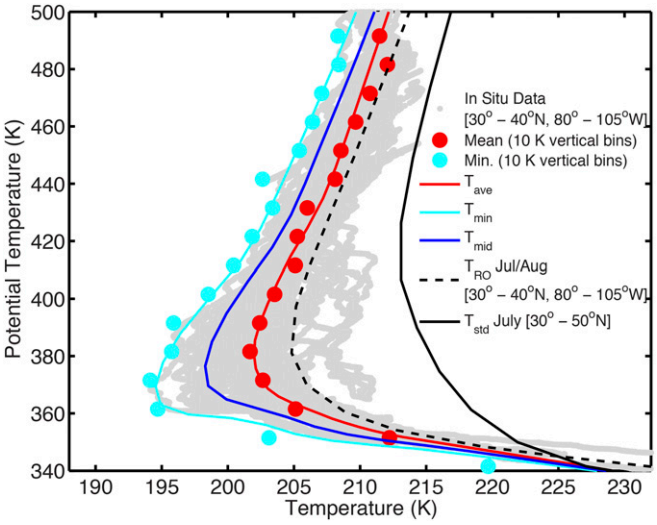

Fig. 4. High spatial resolution in situ temperatures (gray dots) obtained during the NASA SEAC^{4}RS mission over the United States in summer 2013. The distribution in temperature is, in part, due to gravity wave-driven temperature fluctuations. Bin-average profiles for these data are plotted in the red circles, and the smoothed mean profile, T_{ave}, is represented by the solid red line. Similarly, the profile of minimum temperatures, T_{min}, is shown in the cyan circles and line. T_{mid} (blue line) is defined as the temperature profile midway between T_{ave} and T_{min}. The July/August mean of RO temperatures for the same region (black dashed line) demonstrates agreement between the in situ and RO data sets of 2 K or less. Finally, the "standard atmosphere" temperature profile for July that has been used in the AER 2D model, averaged over a region extending from 33°N to 52°N is shown in the solid black line.

Given the remarkable nonlinearity of the heterogeneous catalytic processes that control Cl_y to ClO conversion, the temperature observations are critically important for determining the rate of catalytic loss of ozone; this is particularly true for excursions to low temperatures, given the extremely rapid heterogeneous catalytic conversion of Cl_y to ClO. The AER 2D model employs an empirically derived distribution about the selected temperature at each altitude, with a SD of ∼3 K. For example, with the peak temperature centered at 202 K, ∼7% of the data fall below 197 K (or above 207 K), and <1% are below 195 K (or above 209 K). This temperature distribution has always been intrinsic to the AER 2D model, and it is an important capability of the model to represent a range of temperatures under conditions appropriate to the lower stratosphere in summer over the Great Plains. The high spatial resolution, in situ aircraft observations verify the importance of the temperature distribution function of the AER 2D model.

Dynamics Defining Lower Stratospheric Flow Patterns over the United States in Summer. The NAM creates a situation during July and August that is particularly conducive to the hydration of the lower stratosphere by extremely deep convection. Not only does it steer water vapor from the Gulf of Mexico across Texas and into the western Plains States in the lower atmosphere, it also generates an anticyclone in the upper troposphere and lower stratosphere that causes stratospheric air parcels to dwell markedly longer over North America than if they were advected by a purely zonal flow. This anticyclonic circulation is not stable, however, leading to regular ventilation. Thus, the mean residence time of air over the United States is on the order of a week, with some parcels residing significantly longer (67). The residence time sets the range

of timescales for evaluating ozone loss over this region from one or more of these injections. Evidence that parcels are induced to circulate in a stratospheric anticyclone over North America during summer with convectively injected water vapor retention within the gyre is evident in tracer–tracer (7) and satellite data (68–70).

Two-Dimensional Model Calculations Exploring the Sensitivity of the Rate-Limiting Steps in the Dominant Ozone Loss Processes to Perturbations in Temperature and Water Vapor

Given the remarkable temperature sensitivity and nonlinearity of the heterogeneous catalytic conversion of Cl_y to ClO on sulfate aerosols, and the sensitivity of ozone loss rates to changes in the concentrations of the rate-limiting radicals ClO, BrO, HO_2, and NO_2, we use the AER 2D model (10, 23–26) to determine the impact of observed temperature variability in the presence and absence of convectively injected water vapor on the vertical distribution of the rate-limiting steps of the four major catalytic cycles identified in *Photochemical Framework for Catalytic Ozone Loss*. The AER 2D model calculates all trace gases as functions of latitude, altitude, and season. Long-lived chemical species, such as N_2O and total chlorine (Cl_y) are derived with surface boundary conditions representing the year 2000, and concentrations of short-lived radical species such as ClO and NO_2 are calculated to vary diurnally (10, 23–26). The AER 2D model has established literature values of ozone loss rates across a wide range of conditions. In this analysis, we use the calculated catalytic loss rates to determine the altitude-dependent fractional reduction in ozone. This sensitivity analysis of ozone loss rates to temperature and convective injection of water vapor employs the three temperatures discussed previously.

Fig. 5*A* displays the loss rate of ozone for each of the major catalytic cycles rate-limited by ClO + ClO, ClO + BrO, NO_2 + O, and HO_2 + O_3 for each of the three temperature profiles T_{std}, T_{ave}, and T_{mid} between 12 km and 20 km. All three temperature profiles use the temperature distribution intrinsic to the model as described in *Observations of Temperatures in the Lower Stratosphere*. Fig. 5*A* clarifies the important role that the temperature structure plays in ozone catalytic chemistry. The AER 2D calculations of ozone loss rates using T_{std} (Fig. 5*A*) establish the baseline case against which ozone loss for observed temperatures in the absence and presence of convective input of water can then be compared. Calculations using the observed T_{ave} result in modified but similar loss rates for all four major catalytic cycles compared with the case for T_{std}. However, for the modest decrease in temperature represented by the difference between the observed T_{ave} and T_{mid}, the response of the catalytic cycles is marked. The ClO + ClO loss rate increases by up to four orders of magnitude in the altitude region between 14 km and 16 km, and the ClO + BrO loss rate increases by more than two orders of magnitude. The NO_x catalytic cycle decreases by up to a factor of ~50 as a result of the hydrolysis of N_2O_5 that converts NO_x to nitric acid. The catalytic cycle rate limited by HO_x remains largely unaffected. Catalytic control of ozone thereby transitions from HO_x control to halogen radical control, with an overall increase in the ozone loss rate of two orders of magnitude in the 14- to 16-km range.

Fig. 5*B* addresses the influence of convectively injected water vapor on the same four catalytic cycles for the same three temperature profiles used in Fig. 5*A*. In the model runs with convective injection, water vapor is raised to and maintained at 10 ppmv throughout a 6-km layer in the lower stratosphere between 12 km and 18 km. Although the NEXRAD observations show injection of condensed phase water that is continuous with altitude, the in situ observations of convectively injected water vapor tend to show layers of elevated water that may, in total, span a few kilometers in the days following convective injection. Here we model 6 km of elevated water vapor only to demonstrate the response as a function of altitude, not to imply that a single convective event would distribute 10 ppmv water vapor evenly over this range. Stratospheric water vapor values over the United States in summer significantly higher than 10 ppmv have been observed by MLS and in situ (up to 18 ppmv).

For the case of T_{std}, there is virtually no response to water vapor raised to 10 ppmv (Fig. 5*B*). However, for the temperature

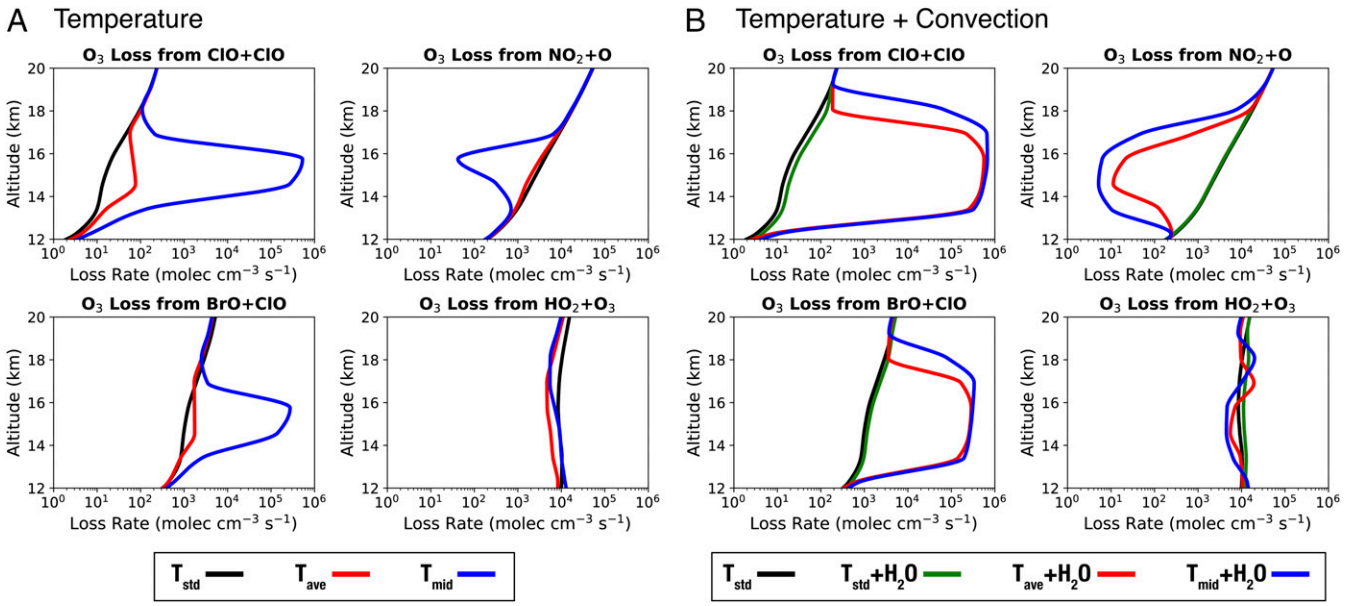

Fig. 5. The response of the four major rate-limiting steps in the catalytic removal of ozone to (*A*) temperature alone and (*B*) temperature plus convective addition of water vapor to a mixing ratio of 10 ppmv. The ozone loss rates, calculated using the AER 2D model, are shown after perturbation of temperature and/or water vapor. The three temperature profiles used in the model are shown in Fig. 4, and the temperature distribution is described in *Observations of Temperatures in the Lower Stratosphere*. A constant 10 ppmv water vapor perturbation between 12 km and 18 km is used to demonstrate the sensitivity in ozone loss rates as a function of altitude (see text).

distribution represented by T_{ave} over the United States in summer, the presence of convected water vapor increases the rate of ozone loss by the ClO + ClO rate-limiting step by over four orders of magnitude between 14 km and 17 km, while increasing the ClO + BrO rate-limiting step by more than two orders of magnitude. Engaging the temperature profile T_{mid} with convection shows similar results to T_{ave}, although extending from 14 km to 18 km. It is clear from comparison of Fig. 5 *A* and *B* that convective injection of water vapor most significantly changes the ozone loss rate for T_{ave}, the temperature distribution most representative of the in situ observations over the United States in summer 2013.

We calculate next the impact on the ozone profile in response to the change in the rate-limiting steps for the three temperature profiles T_{std}, T_{ave}, and T_{mid} in the presence of convective injection. Fig. 6*A* presents the AER 2D model calculated ozone profiles for each of the three temperature profiles 1 wk (the nominal period that a convectively influenced domain resides within the anticyclonic circulation) following convective injection, with water vapor elevated to 10 ppmv from 12 km to 18 km. Here, analogous to Fig. 5*B*, we model 6 km of elevated water to demonstrate the sensitivity of the ozone response as a function of altitude. We do this for a single convective event, recognizing that, on average, over 2,000 convective events extend above ~14 km in a given summer. For the case of T_{std} in Fig. 6*A*, the convective injection has minimal impact on the catalytic loss rate of ozone, and the ozone concentration is unaffected. However, convective injection of water with the observed average temperature, T_{ave}, results in the catalytic loss rate increasing with a corresponding decrease in ozone as a function of altitude. With the introduction of convection in combination with T_{mid}, the altitude-dependent ozone loss increases further.

To quantitatively compare the ozone loss values over the 1-wk period of elevated water vapor shown in Fig. 6*A*, we restrict the altitude range to between 14 km and 18 km and report the results in Fig. 6*B*. This table shows the fractional decreases in ozone between 14 km and 18 km for each of the three temperature profiles in the presence of convectively injected water vapor referenced to T_{std} in the absence of convection. As stated, convective injection does not significantly impact the ozone concentration for T_{std}. The fractional ozone loss for the observed temperature profile, T_{ave}, with enhanced water vapor between 14 km and 18 km is 12%. With the introduction of convection in combination with T_{mid}, the fractional loss of ozone increases to 17%. If we narrow the altitude range for the calculation to 15 km to 17 km, the fractional ozone loss numbers are very similar. Figs. 5 and 6 demonstrate the sensitivity of the altitude-dependent ozone response to the range of observed temperatures in the presence of convectively injected water vapor.

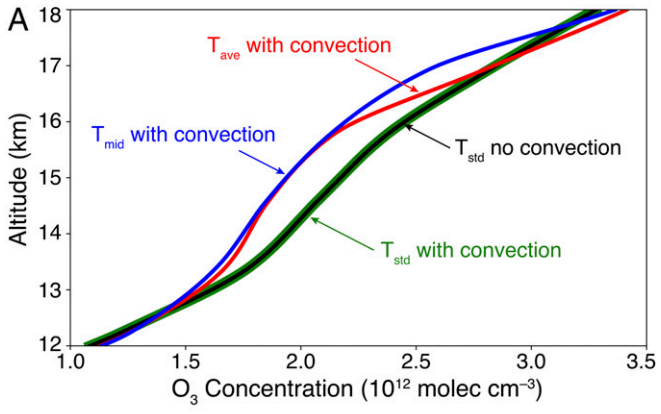

B

Temperature Profile	T_{std}	T_{std}+H_2O	T_{ave}+H_2O	T_{mid}+H_2O
Fractional loss of ozone 14 – 18 km	0%	0%	12%	17%

Fig. 6. (*A*) The modeled response of ozone one week after a single convective injection for three different temperatures and water vapor mixing ratios elevated to 10 ppmv between 12 km and 18 km. The ozone profiles are calculated using the AER 2D model, and the three temperature profiles used in the model are shown in Fig. 4. A constant 10 ppmv water vapor perturbation between 12 km and 18 km is used to demonstrate the sensitivity in ozone concentration as a function of altitude. (*B*) The integrated fractional ozone loss between 14 km and 18 km after 1 wk, calculated as the difference between the modeled ozone profile using T_{std} and the ozone profile using T_{std}, T_{ave}, or T_{mid} with convective addition of water vapor.

Conclusions

The NEXRAD weather radar system observations presented here define stratospheric convective penetration height and frequency over the central United States in summer, demonstrating that, on average, 2,000 storms each summer penetrate into the region of rapidly increasing available inorganic chlorine in the stratosphere. High-accuracy, high spatial resolution observations of the detailed temperature structure of the stratosphere over the United States in summer demonstrate significantly lower temperatures than recognized using lower resolution or zonally averaged datasets, as well as the influence of synoptic scale spatial and structural variability and of gravity wave propagation that can periodically and repeatedly suppress temperatures. These observations are coupled to the framework of photochemical reactions to calculate the rate-limiting loss of ozone resulting from chlorine and bromine free radical catalysis as a function of altitude over the United States in summer. These observations place the stratosphere in a domain capable of initiating heterogeneous catalytic conversion of Cl_y to ClO that serves to increase the rate of catalytic ozone loss.

The analysis of the sensitivity of ozone to different combinations of temperature and convectively injected water vapor is established using two observed temperature profiles in addition to a "standard" temperature profile used in AER 2D model calculations of stratospheric ozone catalytic photochemistry. The sensitivity of ozone to convected water is then determined for each of these three temperature profiles.

When the convective injection of water occurs, the condensed phase, detected by the NEXRAD system, vaporizes into the low relative humidity environment of the stratosphere. The saturation vapor pressure between 14 km and 18 km is in the range of 10 ppmv to 60 ppmv. Considered in a Lagrangian reference frame that tracks the position of the convectively injected domain, any decrease in temperature below the average may impact the extremely rapid kinetics controlling the heterogeneous catalytic conversion of Cl_y to ClO. A mechanism not explicitly addressed here is that the enhancement in water vapor within the convectively affected domain initiates radiative cooling to space that serves to decrease the temperature of the convectively influenced domain at ~0.05 K/d per 1 ppmv additional water vapor.

Thus, the sensitivity of ozone loss over the central United States in summer to the interplay between temperature and water vapor can be manifest within interstitial volume elements, influenced, to varying degrees, by both induced temperature variations and convectively enhanced water vapor. These factors are potentially important for considering impacts on the seasonally averaged lower stratospheric ozone concentrations over the central United States in summer, given the observed temperatures and large number of convective storms over the Great Plains. For observations lacking adequate spatial resolution, the null experiment, defined by ozone concentrations unaffected by heterogeneous catalytic conversion of Cl_y to ClO, may be difficult to establish.

This array of observations, in combination with the resulting amplification of the ozone loss rates by chlorine and bromine

free radical catalysis, advances our understanding of the vulnerability of ozone, specifically over the central United States in summer. Moreover, the analysis of risk now engages the following factors:

i) High spatial resolution, high accuracy in situ observations of temperatures in the stratosphere over the central United States in summer show significantly lower temperatures than recognized using lower-resolution or zonally averaged datasets, an important distinction for model calculations of stratospheric photochemistry. The lowest temperatures observed in situ place the stratosphere in the domain capable of initiating heterogeneous catalytic conversion of Cl_y to ClO that serves to increase the rate of catalytic ozone loss.

ii) Observations from the NEXRAD weather radar system that define the frequency and depth of penetration of convective storms into the stratosphere, as well as the retention of that convection in the anticyclonic gyre that results from the NAM, establish the occurrence of conditions, in concert with the observed temperature structure, that initiate the rapid heterogeneous conversion of Cl_y to ClO and serve to increase the rate of catalytic ozone loss.

iii) Increased forcing of the climate by carbon dioxide and methane leads to cooling of the stratosphere—as would the loss of ozone in the critical altitude region between 14 km and 18 km—thereby potentially shifting the stratosphere toward a temperature domain capable of more frequently initiating heterogeneous catalytic conversion of Cl_y to ClO and, in turn, increasing the rate of ozone loss.

iv) There is significant uncertainty in forecasting the rate of increase in the intensity and frequency of severe storm systems over the central United States in summer resulting from increased forcing of the climate, in the context of the timescale for multidecadal decrease of inorganic chlorine loading (estimated to decrease by ∼50% over the 50 y from 2000 to 2050) resulting from the global ban on CFCs and halons invoked by the Montreal Protocol.

v) In the lower stratosphere, enhanced sulfate loading from volcanic eruptions or overt sulfate addition for climate engineering act in concert with temperature and water vapor in controlling the rate of catalytic ozone loss.

vi) Volcanic eruptions can contain significantly elevated quantities of hydrogen halides in addition to sulfur dioxide. For example, elevated Cl_y was detected in the stratospheric volcanic clouds of El Chichón (1982) and Hekla (2000) (71–74). From petrology, a number of historic eruptions are known to have produced large quantities of HCl and HBr, which would have exceeded peak anthropogenic Equivalent Effective Stratospheric Chlorine that accounts for both chlorine and bromine levels, if even a small fraction of their emissions partitioned to the stratosphere (75–78). A 2016 analysis of MLS satellite observations confirms that the stratospheric injection of halogens is more frequent than previously believed (79).

vii) There is a marked sensitivity of human skin cancer incidence to small increases in UV dosage levels that, in turn, requires a tested and trusted forecast of UV dosage levels over the central United States in the ensuing years and decades.

1. Hanisco TF, et al. (2007) Observations of deep convective influence on stratospheric water vapor and its isotopic composition. *Geophys Res Lett* 34:L04814.
2. Anderson JG, Wilmouth DM, Smith JB, Sayres DS (2012) UV dosage levels in summer: Increased risk of ozone loss from convectively injected water vapor. *Science* 337: 835–839.
3. Homeyer CR, Pan LL, Barth MC (2014) Transport from convective overshooting of the extratropical tropopause and the role of large-scale lower stratosphere stability. *J Geophys Res Atmos* 119:2220–2240.
4. Laing AG, Fritsch JM (1997) The global population of mesoscale convective complexes. *Q J R Meteorol Soc* 123:389–405.
5. Pan LL, et al. (2017) The Convective Transport of Active Species in the Tropics (CONTRAST) experiment. *Bull Am Meteorol Soc* 98:106–128.
6. Gill AE (1980) Some simple solutions for heat-induced tropical circulation. Q *J R Meteorol Soc* 106:447–462.
7. Weinstock EM, et al. (2007) Quantifying the impact of the North American monsoon and deep midlatitude convection on the subtropical lowermost stratosphere using in situ measurements. *J Geophys Res* 112:D18310.
8. Solomon S (1999) Stratospheric ozone depletion: A review of concepts and history. *Rev Geophys* 37:275–316.
9. Fahey DW, et al. (1993) In situ measurements constraining the role of sulphate aerosols in mid-latitude ozone depletion. *Nature* 363:509–514.
10. Salawitch RJ, et al. (2005) Sensitivity of ozone to bromine in the lower stratosphere. *Geophys Res Lett* 32:L05811.
11. Solomon S, et al. (1998) Ozone depletion at mid-latitudes: Coupling of volcanic aerosols and temperature variability to anthropogenic chlorine. *Geophys Res Lett* 25: 1871–1874.
12. Canty T, Mascioli NR, Smarte MD, Salawitch RJ (2013) An empirical model of global climate – Part 1: A critical evaluation of volcanic cooling. *Atmos Chem Phys* 13: 3997–4031.
13. Tilmes S, Garcia RR, Kinnison DE, Gettelman A, Rasch PJ (2009) Impact of geoengineered aerosols on the troposphere and stratosphere. *J Geophys Res* 114:D12305.
14. McCormack CG, et al. (2016) Key impacts of climate engineering on biodiversity and ecosystems, with priorities for future research. *J Integr Environ Sci* 13:103–128.
15. Crutzen PJ (2006) Albedo enhancement by stratospheric sulfur injections: A contribution to resolve a policy dilemma? *Clim Change* 77:211–220.
16. Pitari G, et al. (2014) Stratospheric ozone response to sulfate geoengineering: Results from the Geoengineering Model Intercomparison Project (GeoMIP). *J Geophys Res* 119:2629–2653.
17. Dykema JA, Keith DW, Anderson JG, Weisenstein D (2014) Stratospheric controlled perturbation experiment: A small-scale experiment to improve understanding of the risks of solar geoengineering. Philos Trans R Soc Lond A Phys *Eng Sci* 372:20140059.
18. Weisenstein DK, Keith DW, Dykema JA (2015) Solar geoengineering using solid aerosol in the stratosphere. *Atmos Chem Phys* 15:11835–11859.
19. Feng Z, et al. (2016) More frequent intense and long-lived storms dominate the springtime trend in central US rainfall. *Nat Commun* 7:13429.
20. Tippett MK, Lepore C, Cohen JE (2016) More tornadoes in the most extreme U.S. tornado outbreaks. *Science* 354:1419–1423.
21. Diffenbaugh NS, Scherer M, Trapp RJ (2013) Robust increases in severe thunderstorm environments in response to greenhouse forcing. *Proc Natl Acad Sci USA* 110: 16361–16366.
22. Trapp RJ, Hoogewind KA (2016) The realization of extreme tornadic storm events under future anthropogenic climate change. *J Clim* 29:5251–5265.
23. Weisenstein DK, et al. (1997) A two-dimensional model of sulfur species and aerosols. *J Geophys Res* 102:13019–13035.
24. Weisenstein DK, et al. (1998) The effects of sulfur emissions from HSCT aircraft: A 2-D model intercomparison. *J Geophys Res* 103:1527–1547.
25. Ko MKW, Sze N-D, Scott CJ, Weisenstein DK (1997) On the relation between stratospheric chlorine/bromine loading and short-lived tropospheric source gases. *J Geophys Res* 102:25507–25517.
26. Rinsland CP, et al. (2003) Post-Mount Pinatubo eruption ground-based infrared stratospheric column measurements of HNO_3, NO, and NO_2 and their comparison with model calculations. *J Geophys Res* 108:4437.
27. Weinstock MA (1995) Overview of ultraviolet radiation and cancer: What is the link? How are we doing? *Environ Health Perspect* 103:251–254.
28. Diepgen TL, Mahler V (2002) The epidemiology of skin cancer. *Br J Dermatol* 146:1–6.
29. Matsumura Y, Ananthaswamy HN (2004) Toxic effects of ultraviolet radiation on the skin. *Toxicol Appl Pharmacol* 195:298–308.
30. Duthie MS, Kimber I, Norval M (1999) The effects of ultraviolet radiation on the human immune system. *Br J Dermatol* 140:995–1009.
31. Tevini M, Teramura AH (1989) UV-B effects on terrestrial plants. *Photochem Photobiol* 50:479–487.
32. Molina MJ, Rowland FS (1974) Stratospheric sink for chlorofluoromethanes: Chlorine atom-catalysed destruction of ozone. *Nature* 249:810–812.
33. Solomon S, Garcia RR, Rowland FS, Wuebbles DJ (1986) On the depletion of Antarctic ozone. *Nature* 321:755–758.
34. Molina LT, Molina MJ (1987) Production of Cl_2O_2 from the self-reaction of the ClO radical. *J Phys Chem* 91:433–436.
35. McElroy MB, Salawitch RJ, Wofsy SC, Logan JA (1986) Reductions of Antarctic ozone due to synergistic interactions of chlorine and bromine. *Nature* 321:759–762.
36. Anderson JG, Toohey DW, Brune WH (1991) Free radicals within the Antarctic vortex: The role of CFCs in Antarctic ozone loss. *Science* 251:39–46.
37. Brune WH, Toohey DW, Anderson JG, Chan KR (1990) In situ observations of ClO in the arctic stratosphere: ER-2 aircraft results from 59°N to 80°N latitude. *Geophys Res Lett* 17:505–508.
38. Stimpfle RM, et al. (1999) The coupling of $ClONO_2$, ClO, and NO_2 in the lower stratosphere from in situ observations using the NASA ER-2 aircraft. *J Geophys Res* 104:26705–26714.
39. Newman PA, et al. (2002) An overview of the SOLVE/THESEO 2000 campaign. *J Geophys Res* 107:8259.
40. Hanisco TF, et al. (2002) Quantifying the rate of heterogeneous processing in the Arctic polar vortex with in situ observations of OH. *J Geophys Res* 107:8278.

41. Stimpfle RM, Wilmouth DM, Salawitch RJ, Anderson JG (2004) First measurements of ClOOCl in the stratosphere: The coupling of ClOOCl and ClO in the arctic polar vortex. *J Geophys Res* 109:D03301.
42. Wilmouth DM, et al. (2006) Evolution of inorganic chlorine partitioning in the arctic polar vortex. *J Geophys Res* 111:D16308.
43. Manney GL, et al. (2011) Unprecedented Arctic ozone loss in 2011. *Nature* 478: 469–475.
44. Solomon S, et al. (1996) The role of aerosol variations in anthropogenic ozone depletion at northern midlatitudes. *J Geophys Res* 101:6713–6727.
45. Shi Q, Jayne JT, Kolb CE, Worsnop DR, Davidovits P (2001) Kinetic model for reaction of $ClONO_2$ with H_2O and HCl and HOCl with HCl in sulfuric acid solutions. *J Geophys Res* 106:24259–24274.
46. Drdla K (2005) Temperature thresholds for polar stratospheric ozone. *Eos Trans. AGU* 86:Abstract A31D-03.
47. Drdla K, Müller R (2012) Temperature thresholds for chlorine activation and ozone loss in the polar stratosphere. *Ann Geophys* 30:1055–1073.
48. Burkholder JB, et al. (2015) *Chemical Kinetics and Photochemical Data for Use in Atmospheric Studies: Evaluation No. 18* (Jet Propul Lab, Pasadena, CA), Vol 15-10.
49. Wennberg PO, et al. (1994) Removal of stratospheric O_3 by radicals: In situ measurements of OH, HO_2, NO, NO_2, ClO, and BrO. *Science* 266:398–404.
50. Homeyer CR (2014) Formation of the enhanced-V infrared cloud-top feature from high-resolution three-dimensional radar observations. *J Atmos Sci* 71:332–348.
51. Solomon DL, Bowman KP, Homeyer CR (2016) Tropopause-penetrating convection from three-dimensional gridded NEXRAD data. *J Appl Meteorol Climatol* 55:465–478.
52. Toon OB, et al. (2016) Planning, implementation, and scientific goals of the Studies of Emissions and Atmospheric Composition, Clouds and Climate Coupling by Regional Surveys (SEAC^{4}RS) field mission: Planning SEAC^{4}RS. *J Geophys Res Atmos* 121: 4967–5009.
53. Homeyer CR, Kumjian MR (2015) Microphysical characteristics of overshooting convection from polarimetric radar observations. *J Atmos Sci* 72:870–891.
54. Bigelbach BC, Mullendore GL, Starzec M (2014) Differences in deep convective transport characteristics between quasi-isolated strong convection and mesoscale convective systems using seasonal WRF simulations. *J Geophys Res Atmos* 119: 11445–11455.
55. Bonne GP, et al. (2000) An examination of the inorganic chlorine budget in the lower stratosphere. *J Geophys Res* 105:1957–1971.
56. Marcy TP, et al. (2004) Quantifying stratospheric ozone in the upper troposphere with in situ measurements of HCl. *Science* 304:261–265.
57. Schwartz MJ, et al. (2013) Convectively injected water vapor in the North American summer lowermost stratosphere. *Geophys Res Lett* 40:2316–2321.
58. Randel WJ, et al. (2012) Global variations of HDO and HDO/H_2O ratios in the upper troposphere and lower stratosphere derived from ACE-FTS satellite measurements. *J Geophys Res* 117:D06303.
59. Sayres DS, et al. (2010) Influence of convection on the water isotopic composition of the tropical tropopause layer and tropical stratosphere. *J Geophys Res* 115:D00J20.
60. Leroy SS, Ao CO, Verkhoglyadova O (2012) Mapping GPS radio occultation data by Bayesian interpolation. *J Atmos Oceanic Technol* 29:1062–1074.
61. Hajj GA, et al. (2002) A technical description of atmospheric sounding by GPS occultation. *J Atmos Sol Terr Phys* 64:451–469.
62. Ern M, Preusse P, Alexander MJ, Warner CD (2004) Absolute values of gravity wave momentum flux derived from satellite data. *J Geophys Res* 109:D20103.
63. Alexander MJ, et al. (2008) Global estimates of gravity wave momentum flux from High Resolution Dynamics Limb Sounder observations. *J Geophys Res* 113:D15S18.
64. Wang L, Alexander MJ (2010) Global estimates of gravity wave parameters from GPS radio occultation temperature data. *J Geophys Res* 115:D21122.
65. Maycock AC, Shine KP, Joshi MM (2011) The temperature response to stratospheric water vapour changes. *Q J R Meteorol Soc* 137:1070–1082.
66. Dykema JA, Keith DW, Keutsch FN (2016) Improved aerosol radiative properties as a foundation for solar geoengineering risk assessment. *Geophys Res Lett* 43:7758–7766.
67. Koby TR (2016) Development of a trajectory model for the analysis of stratospheric water vapor. PhD thesis (Harvard Univ, Cambridge, MA).
68. Dessler AE, Sherwood SC (2004) Effect of convection on the summertime extratropical lower stratosphere. *J Geophys Res* 109:D23301.
69. Sun Y, Huang Y (2015) An examination of convective moistening of the lower stratosphere using satellite data. *Earth Space Sci* 2:320–330.
70. Randel WJ, Zhang K, Fu R (2015) What controls stratospheric water vapor in the NH summer monsoon regions? *J Geophys Res Atmos* 120:7988–8001.
71. Hunton DE, et al. (2005) In-situ aircraft observations of the 2000 Mt. Hekla volcanic cloud: Composition and chemical evolution in the arctic lower stratosphere. *J Volcanol Geotherm Res* 145:23–34.
72. Rose WI, et al. (2006) Atmospheric chemistry of a 33–34 hour old volcanic cloud from Hekla volcano (Iceland): Insights from direct sampling and the application of chemical box modeling. *J Geophys Res* 111:D20206.
73. Millard GA, Mather TA, Pyle DM, Rose WI, Thornton B (2006) Halogen emissions from a small volcanic eruption: Modeling the peak concentrations, dispersion, and volcanically induced ozone loss in the stratosphere. *Geophys Res Lett* 33:L19815.
74. Mankin WG, Coffey MT (1984) Increased stratospheric hydrogen chloride in the El Chichon cloud. *Science* 226:170–172.
75. Cadoux A, Scaillet B, Bekki S, Oppenheimer C, Druitt TH (2015) Stratospheric ozone destruction by the Bronze-Age Minoan eruption (Santorini volcano, Greece). *Sci Rep* 5:12243.
76. Vidal CM, et al. (2016) The 1257 Samalas eruption (Lombok, Indonesia): The single greatest stratospheric gas release of the Common Era. *Sci Rep* 6:34868.
77. Kutterolf S, et al. (2015) Bromine and chlorine emissions from Plinian eruptions along the Central American Volcanic Arc: From source to atmosphere. *Earth Planet Sci Lett* 429:234–246.
78. Kutterolf S, et al. (2013) Combined bromine and chlorine release from large explosive volcanic eruptions: A threat to stratospheric ozone? *Geology* 41:707–710.
79. Carn SA, Clarisse L, Prata AJ (2016) Multi-decadal satellite measurements of global volcanic degassing. *J Volcanol Geotherm Res* 311:99–134.